

# Kinetic roughening with anisotropic growth rules

Raffaele Cafiero<sup>1</sup>

<sup>1</sup>*L.P.M.M.H. Ecole Supérieure de Physique et de Chimie Industrielles, 10, rue Vauquelin, 75231 Paris CEDEX 05 France*

Inspired by the chemical etching processes, where experiments show that growth rates depending on the local environment might play a fundamental role in determining the properties of the etched surfaces, we study here a model for kinetic roughening which includes explicitly an anisotropic effect in the growth rules. Our model introduces a dependence of the growth rules on the local environment conditions, i.e. on the local curvature of the surface. Variables with different local curvatures of the surface, in fact, present different quenched disorder and a parameter  $P$  (which could represent different experimental conditions) is introduced to account for different time scales for the different class of variables. We show that the introduction of this *time scale separation* in the model leads to non-universal roughness properties. The interplay between anisotropy and the non-universality and the dependence of critical properties on parameter  $p$  is investigated as well as the relationship with the known universality classes.

PACS: 05.65.b, 68.35.Ja, 81.65.Cf

## I. INTRODUCTION

In the last years the study of physical phenomena characterized by a degree of self-organization [1], has attracted a lot of interest. These models are usually cellular automata models defined on a discretized lattice, with a growth rule that can be either stochastic, when the inhomogeneities in the system change with a time scale smaller than the characteristic time scale of the dynamical evolution (noise), or deterministic with a quenched disorder which accounts for the effect of inhomogeneities inside a solid medium. Both kind of dynamical rules are characterized by an evolution towards an attractive fixed point in which scale free fluctuations in time and space are present [2].

The problem of kinetic roughening belongs to this class of models. It received recently an increasing interest in relation with non-equilibrium growth models [3] and in view of its practical applications: Chemical Vapor Deposition (CVD) [4] and electro-chemical deposition [5] are just two examples.

In this perspective, one is interested in identifying the dynamic universality classes of kinetic roughening processes and several models have been defined starting from the models falling in the universality class of the Kardar-Parisi-Zhang (KPZ) equation [6]. This equation describes the properties of an interface  $h(x, t)$  driven by a stochastic noise and gives a roughness exponent  $\chi = 0.5$ . Other models are more suitable to describe the propagation of interfaces in random media, i.e. with a quenched disorder. These models are driven by an extremal dynamics. In this class fall the so-called Sneppen model [7] (in [7] referred as model B) and the pinning model by directed percolation [8], which predict a roughness exponent equal to  $\chi = 0.63$ . These models produce self-affine surfaces. Recently, a model has been introduced to describe some etching experiments, which leads to the formation of self-similar (fractal) structures, and which has been shown to fall in the percolation universality class

[9]. Many experiments on surface roughening [10–12], however, as well as experiments on chemical etching [13] produce self-affine surfaces instead of self-similar ones. In this paper, we will focus on kinetic roughening phenomena leading to *self-affine* ( $\chi < 1$ ) surfaces.

We recall that the roughness exponent is defined by the ensemble averaged width of the interface as  $W(l, t) = \langle (h(x, t) - \langle h(x, t) \rangle)^2 \rangle^{1/2} \sim l^\chi f(t^{1/z}/l)$  where  $z$  is the so-called dynamical exponent, the angular brackets denote the average over all segments of the interface of length  $l$  and over all different realizations.  $f$  is a scaling function such that  $f(y) \sim y^\chi$  for  $y \ll 1$  and  $f(y) = \text{const.}$  for  $y \gg 1$ . The exponent  $\beta = \chi/z$  describes the transient roughening, during which the surface evolves from the initial condition toward the final self-affine structure.

In spite of the strong universality exhibited by the KPZ and Sneppen models, in many experimental studies one measures values of  $\chi$  which are above the ones predicted by both the KPZ and Sneppen universality classes. To give some examples, we remember the experimental studies of paper burning for which one gets  $\chi = 0.70 \pm 0.03$  [10], or the propagation of a forced fluid front in a porous medium, which exhibits a roughness exponent  $\chi = 0.73 \pm 0.03$  [11] and  $\chi = 0.88 \pm 0.08$  [12].

In this paper we propose a generalized model for kinetic roughening characterized by anisotropic growth rules and non-universal self-organized critical properties.

Some results presented here have been already briefly reported on in a letter [13]. In this long paper we give a detailed, complete description of our previous work. Moreover, we present a set of new numerical results with respect to [13].

The idea underlying the model is that some experimental parameters, although they do not visibly affect the criticality of the roughening phenomena, can determine different values for the critical exponents like the roughness exponent  $\chi$ . In particular we consider a model which includes explicitly an anisotropy factor, say a growth rule dependent on the local environment of the growing site.

The model thus presents a complex interplay between a global equilibrium and the conditions of a local dynamics. This choice is motivated by the observation of roughening phenomena occurring in etching processes which represent an important tool either in academic research or in device technology. Their importance is related to the preparation of single-crystal samples of desired dimensions, shapes and orientations. Etching is usually applied to obtain desired mesas and grooves in semiconductors wafers and multilayers [14].

In the same field, although in a different context, etching processes are used to produce textured optical sheets, which allow to exploit the light trapping by total internal reflection to increase the effective absorption in the indirect-gap semiconductors crystalline silicon. Light trapping, originally suggested to increase the response speed of silicon photo-diodes while maintaining high quantum efficiency in the near-infrared, was later indicated as an important benefit for solar cells [14].

The general suffix *etching* indicates the ensemble of operations which involve the removal of materials by expending energy either by mechanical, thermal or chemical means. In ref. [13] the authors focused their attention on chemical etching processes as a reference point to formulate the model. One of the most important properties of these processes is represented by the intrinsic anisotropy [15,16] of the etch rates. For instance in samples of crystalline silicon etched in solutions of aqueous potassium-hydroxide (K-OH) with isopropil alcohol (IPA), depending on the concentration of the etchant and the temperature, the (111) direction etches slower than the others by a factor which can be of order 100 or more [17]. The degree of anisotropy affects the properties of the surface, which turns out to be rough with a non-universal roughness exponent.

Although the definition of the model is very general we will briefly consider the chemistry of the etching process in order to exhibit a physical framework that allows to understand the meaning of the definitions and their interpretation.

The disorder in the etching process is related to the impurities in the lattice. Such impurities, e.g. vacant atoms, reduce the binding energy of atoms nearby the vacancy. By assigning to each site (atom) of our lattice a random number  $x_i$  we assume that a distribution of vacancies, or other kinds of impurities, is present in the system, and this induces fluctuations in the binding energy of atoms due to this disorder. If we assume to be in a condition of slow dynamics, that is to say the driving field (which in our case is represented by the concentration of etchant) tends to zero [18], we can look at the etching as an extremal process, where the etchant dissolves the atom with the smallest binding energy. This is correct for low etchant concentrations and corresponds actually to the situation experimentally more interesting, in which rough surfaces are produced.

The observed non-universal behavior of the roughening properties of the etched surfaces suggests that a mi-

croscopic model for the physical process should contain some tunable parameters (at least one), whose values would reproduce the experimental conditions (type of etchant, concentration, temperature). In our model, the anisotropy is introduced by a phenomenological tunable parameter,  $p$ , which distinguishes sites with a different local environment.

Let us look at the meaning of  $p$  in the case of etching. If we represent the crystalline lattice of the silicon on a two-dimensional plane we can imagine a square lattice where (see Fig.(1)) the atoms can be found in each of the four positions marked in figure by the letters  $a - d$ . The four positions correspond to different oxidation states: from the situation ( $c$ ) (oxidation number 0) which occurs only in the bulk, to the situation ( $d$ ) (oxidation number  $-3$ ). Note that all the surface atoms are passivated by hydrogen atoms. The atoms in the positions ( $a$ ) and ( $b$ ), corresponding respectively to the oxidation numbers  $-2$  and  $-1$  (two and one heteropolar bonds, i.e. Si-H bonds), play an important role in explaining, at least from a heuristic point of view, the origin of the anisotropy in the etched rates [16]. The parameter  $p$  quantifies the ratio of the etch rates between the sites in the positions ( $a$ ) and ( $b$ ). The basic idea is that in the (111)-plane of silicon, there is only one heteropolar bond per silicon atom. Therefore there are three bonds to break for dissolution, while other planes (except the (110)) have more than one heteropolar bonds and accordingly a smaller number of bonds must be broken.

The paper is organized as follows. In section II we describe in detail the model and the setup of numerical simulations. In section III we present and discuss the numerical results in relation with the Sneppen model A and B universality classes. In section IV we briefly describe the results of a simple experiment reported in [13]. The results of this experiment although non definitive, seem to support qualitatively the non universality of the roughening exponent obtained with our model. More refined experiments are however needed to give a quantitative support to the application of our model to the study of etching phenomena. In section V a discussion of the results and some conclusions are drawn together with a planning of future researches.

## II. THE MODEL

We give now a detailed definition of the model. The model is defined on a square  $2D$  lattice tilted at  $45^\circ$  (see fig. 1). We consider a  $1 + 1$  dimensional interface  $h(x) = h(x, t)$  with  $x = 1, 2, \dots, L$ , where  $L$  is the linear extension of the interface in the  $x$  direction. The initial condition for the dynamical evolution of this interface is given by:  $h(2x, 0) = 1 \forall x \in [1, L/2]$  and  $h(2x - 1, 0) = 0 \forall x \in [1, L/2]$ , in order to have both classes of variables (lattice planes) participating to the dynamics from the beginning, but different initial con-

ditions do not change the properties of the model. The interface, which satisfies locally the conditions [19]

$$\begin{aligned} |h(x, t) + 1 - h(x-1, t)| &\leq 1, \\ |h(x, t) + 1 - h(x+1, t)| &\leq 1, \end{aligned} \quad (1)$$

contains two classes of random variables that correspond to two separate classes of sites: The sites ( $M$ ) for which it holds  $\nabla^2 h > 0$  (called minimum sites) which are, microscopically, the atoms with two heteropolar bonds, and the sites on a slope (slope ( $S$ ) sites) for which one has  $\nabla^2 h = 0$ . These last sites correspond microscopically to atoms with one heteropolar bond. To each class of sites is assigned a class of Gaussian distributed uncorrelated random variables which mimic the disorder, and represents physically, for the case of etching, the binding energy of atoms:

$$\eta(x, h) \in \begin{cases} [0 : 0.5] & \text{if } x \text{ is such that } \nabla^2 h = 0 \\ (0.5 : 1] & \text{if } x \text{ is such that } \nabla^2 h > 0. \end{cases} \quad (2)$$

The sites with  $\nabla^2 h < 0$ , for which all the chemical bonds are homopolar, i.e. Si-Si, do not take part to the dynamics and they have assigned a zero value of the random variable. Periodic boundary conditions are assumed along the  $x$  direction.

The system evolves by updating the site  $i^*$  with the largest r.v. in one of the two classes of sites chosen, at its turn, with a probability  $p$ . One thus updates with probability  $p$  a site ( $S$ ) and with probability  $1 - p$  a site ( $M$ ) according to the rules (see. fig(2)):

- (1)  $h(i^*, t+1) = h(i^*, t) + 2, \quad \eta(i^*, h(i^*, t+1), t+1) = 0;$
- (2) Updating all the sites necessary to make satisfied the conditions 1 (this phase is assumed to be instantaneous with respect to extremal dynamics);
- (3) Updating of the random variables for the sites which changed their class of belonging. In particular  $\eta(x, h, t+1) = 1/2 * RAN$  if  $\eta(x, h, t) = 0$  and  $\eta(x, h, t+1) = \eta(x, h, t) + 1/2$  if  $\eta(x, h, t) \neq 0$ , where  $RAN$  is a random value between 0 and 1;
- (4) Updating of the random variables of the sites which have changed their height but which did not change their class of belonging, (sites  $S$  only):  $\eta(x, h, t+1) = 1/2 * RAN$ .

The parameter  $p$  can vary in the range  $[0 : 1/2]$ . If we define  $t_S$  as the characteristic time scale for  $S$  variables and  $t_M$  the characteristic time scale for  $M$  variables one has:

$$r = \frac{t_M}{t_S} = \frac{p}{1-p} \quad (3)$$

The growth of the interface, in the etching process, represent the invasion of the etchants into the silicon wafer. From this point of view the updating of the sites ( $S$ )

mimics the etching of the (111) planes and the updating of the ( $M$ ) sites the etching in the (100) direction. For  $p = 1/2$  all the sites which take part to the dynamics are equivalent and there is no anisotropy ( $r = 1$ ), whereas the case  $p = 0$  corresponds to the maximal anisotropy in which  $v_{(111)}/v_{(100)} = r = 0$ , where  $v_{(111)}$  and  $v_{(100)}$  are the etch rates in the corresponding directions.

Our model can be viewed as a variation of the Sneppen model for quenched surface growth, where two important elements are added: 1) The anisotropy in the distribution of the quenched random field, depending on the local characteristics of the growing surface: 2) a time scale separation for the dynamical evolution of the two classes of variables ( $S$  sites and  $M$  sites), which is tuned by the parameter  $p$ .

### III. NUMERICAL RESULTS

We have studied this cellular automata by numerical simulations in order to analyze its dynamical roughening properties. The size we choose for the numerical simulations is  $L = 2048$ . We have checked that results do not change for larger sizes and we compare several sizes in order to obtain reliable data for the roughness exponents. For each value of the parameter  $p$  (we have considered  $p = 0.0, 0.02, 0.2, 0.5$ ) we have computed the growth exponent  $\beta$ , which rules the time evolution of the width  $W(t)$  of the surface ( $W(t) \sim t^\beta$ ) before the stationary critical state is reached, and the roughness exponent  $\chi$ , which gives the scaling of the width of the surface ( $W(l) \sim l^\chi$ ), in the stationary state. The stationary state is called self-organized in that it is reached spontaneously by the system independently of the initial conditions. This self-organization is confirmed by an analysis of the temporal evolution of the distribution of quenched variables (the histogram  $\Phi_t(\eta)$ ). To characterize temporal correlations in the dynamics and check that the asymptotic state is critical, we studied the distribution of the avalanches in the asymptotic state. As an independent check of the nonuniversality of the roughness properties of the model, we have studied numerically the power spectrum  $S(k)$  of the height profile.

To ensure that the system is in the stationary state, we studied the behavior of the  $n$ -th moments (for  $n = 3, 4, 5$ ) of  $h(x, t)$  normalized to second momentum:

$$m_n(t) = \frac{\langle \sum_i (h(i, t) - \bar{h}(t))^n \rangle}{(\langle \sum_i (h(i, t) - \bar{h}(t))^2 \rangle)^{\frac{n}{2}}}, \quad (4)$$

where  $\bar{h}(t)$  is the mean surface height at time  $t$ . We get that, after a transient, all the odd moments vanish and the even ones tend to constant values (see figg. 3-5). In particular the condition for the skewness  $m_3 = 0$  (fig. 3), which characterizes the stationary critical state [7], is realized after about  $10^3$  time steps per site, independent of the value of  $p$ . These results imply that

the higher moments of the variable  $h(x, t) - \langle h \rangle$  scale in a trivial way (they are powers of the second moment), and after the transient the probability distribution of the variable  $h(x, t)$ , which can be viewed as a random variable, is Gaussian. The amplitude of the normalized even moments  $m_{2n}$ , in the asymptotic stationary state, characterizes the roughness properties of the interface.

For each value of  $p$ ,  $10^2$  simulations lasting  $10^7$  time steps have been performed. In Table I we report the measured values for the exponents  $\chi$  and  $\beta$ . Fig.(6) shows the scaling behavior of  $W(l)$  for different values of  $p$ . One can see that  $\chi$  varies continuously from the value  $\chi = 0.93(2)$  (for  $p = 0.0$ , i.e. maximal anisotropy) corresponding to Sneppen model A [7], to  $\chi = 0.63(2)$  (for  $p = 0.5$ , i.e. no anisotropy) corresponding to the Sneppen model B. The value of  $\chi$  for  $p = 0.0$  is clearly affected by a finite-size effect. We checked how this value tends, in the limit  $L \rightarrow \infty$ , to the value  $\chi = 1.0$  found for Sneppen model A [7] (see fig. 7). In fig. 8 we show the same analysis as in Fig. 7, but for  $p = 0.02, 0.2$ . One can see that, apart a saturation effect, which shifts to higher values of  $l$  as the system size is increased, the surface exhibits roughness properties with an exponent  $\chi = 0.76(2)$ , well away from both values 1 and 0.63 corresponding to the trivial limits of the Sneppen models A and B respectively [7]. Finally in Fig. 9 we study the  $p = 0.2$  case, for which we get a good fit, away from the saturation region, giving  $\chi = 0.65(2)$ . These results corroborate the idea that the observed non-universal roughness properties of our model are a genuine effect, and not some sort of cross-over effect. The exponent  $\beta$  shows, instead, a more universal behavior, assuming a nearly stable value around 0.95 for all values of  $p$  (see Table I). This is not surprising, since Sneppen models A and B have similar values of  $\beta$ , respectively 0.95(5) and 0.9(1), as reported in [7].

We have also studied the time evolution of the distribution of random variables on the invading interface (the histogram  $\Phi_t(\eta)$ , where  $\eta$  is a generic value for  $\eta(x, h)$ ), which is of great importance for models with extremal dynamics. The results of the simulation are shown in figg. 10-13. One can see that  $\Phi_t(\eta)$  self-organizes, for  $p \neq 0$ , after about  $10^5$  time steps, into a distribution that is the superposition of two theta functions, one for each class of variables, each one characterized by a critical threshold  $p_c(p)$  depending on the parameter  $p$ . The meaning of these thresholds is that only  $S$  variables larger than  $\eta_c^S$  and  $M$  variables larger than  $\eta_c^M$  can grow [2]. For  $p = 0$ , instead, the histogram has no self-organized critical state (fig. 10). Looking carefully at fig. 10 we can see that, while in the initial transient there are a few  $S$  sites, in the asymptotic state most sites are  $S$  sites. In fact nearly all variables larger than 0.5 (the  $M$  variables) are disappeared. This observation agrees with the actual structure of the surface, which is composed by very big pyramids (fig. 14), with a roughness exponent  $\chi \simeq 1$ . This picture is confirmed by the acceptance profile  $a(\eta)$ , which is shown in fig. 15. As in the Bak and Sneppen

model, the acceptance profile (that is to say the distribution of the values of all updated quenched variables up to the actual time) exhibits correlation properties (it is not flat), reflecting temporal correlations in the dynamics. But, while the acceptance profile for  $S$  variables is quite similar to that of the BS model, going to zero linearly at  $p_c$ , the acceptance profile for  $M$  variables has a more complicated behavior. This difference originates maybe from the fact that  $S$  variables ( $\eta \in [0.5, 1]$ ) can turn into  $M$  ( $\eta \in [0, 0.5]$ ) variables during the dynamics of the system, while  $M$  variables cannot become  $S$  variables. Moreover,  $S$  variables can have developed correlations before the transition to  $M$  variable and this affects the shape of  $a(\eta)$  for  $\eta \in [0.5, 1]$ . This might account for the linear part of the acceptance profile of  $M$  variables, around  $\eta = 1$ , but the non linear part is more puzzling. The coupling between  $S$  variables and  $m$  variables could play a role in this behavior, too, but at the moment we have no clear explanation of it. From the  $a(\eta)$  we can get a good estimation of the critical thresholds  $\eta_c^S$  and  $\eta_c^M$  for different values of  $p$  (see Table II).

The stationary state is characterized by a constant ratio between  $S$  sites and  $M$  sites, that is to say the evolution equation for the densities  $\rho_S$  and  $\rho_M$  of sites  $S$  and  $M$  respectively, have an attractive fixed point in the stationary state (see fig. 16a-d), with the asymptotic values of  $\rho_S, \rho_M$  depending on the parameter  $p$ . One interesting observation is that, even in the case  $p = 0$ , that is to say only  $M$  sites can be selected by the extremal dynamical rule, there is a stationary state for the system with  $\rho_S \neq 0$ . This is due to the particular geometry of the lattice, for which the growth of an  $M$  site implies the creation or annihilation of some  $S$  sites. In other words, there cannot be surfaces without slopes ( $S$  sites).

The roughness exponent accounts for scale free spatial fluctuations in the interface profile. In order to characterize the eventual scale free fluctuations in the dynamical evolution of the system at its asymptotic critical state, that is to say long range temporal correlations, we have studied the avalanche distribution. An avalanche is defined as a sequence of causally connected elementary growth events. For the class of models with quenched disorder and an extremal dynamics to which our model belongs, the initiator of a critical, scale invariant, avalanche is identified in the critical state by a site with quenched variable  $\eta_c^M(p)$  or  $\eta_c^S(p)$  (respectively for an  $M$  initiator and for an  $S$  initiator). The values of  $\eta_c^M$  and  $\eta_c^S$  for different values of  $p$  can be obtained by the asymptotical histogram distributions shown in figg. 10-13. In our case there are two classes of variables, the  $S$  and  $M$  sites, and two possible initiators for an avalanche. We call the avalanches that start with an  $S$  site,  $S$ -avalanches, and the avalanches that start with an  $M$  site,  $M$ -avalanches. An avalanche lasts when a variable which has been updated before the growth of the initiator is selected by the extremal dynamics. The statistics of off-critical avalanches has been shown to have the form [2,20]:

$$P^X(s; \eta) = s^{-\tau_X} f_X(|\eta - \eta_c^X| s^{\sigma_X}) \quad (5)$$

where  $X = S, M$ , and  $\eta$  is the initiator of an  $X$ -avalanche. This distribution becomes a pure power law for  $\eta = \eta_c^X$ . In the limit  $t \rightarrow \infty$  the system self-organizes into the critical state  $\eta = \eta_c^X$ , and the (normalized) avalanche size distribution becomes:

$$P^X(s; \eta_c^X) = \frac{s^{-\tau_X}}{\sum_{s=1}^{\infty} s^{-\tau_X}} \quad (6)$$

We have performed a set of about  $10^3$  realizations of size  $L = 8192$ , lasting each one  $2 \times 10^6$  time steps, and collected the statistics of  $S$  and  $M$  avalanches over the last  $10^6$  time steps, for  $p = 0.02, 0.2, 0.5$ . These simulations required about 2 months of CPU time on our computers (a network of DEC alpha machines with clocks going from 266Mhz to 500Mhz), and are at the best of our computation possibilities. To reduce numerical problems connected with the approximation on  $\eta_c^M, \eta_c^S$ , we used an alternative definition of critical avalanches in models with extremal dynamics, which resides on the causal relation between updated sites inside an avalanche (for details on the definition of critical avalanches see [21–23]). The results are shown in figg. (17), (18). Even after this big computational effort, our numerical results are still a bit noisy. In particular the statistic of  $S$  avalanches for  $p = 0.02$  is really poor. This is due to the fact that for small  $p$  values most of sites selected by the dynamics are  $M$  sites. However, we can observe a quite clear power law behavior for both the  $S$ -avalanches and  $M$ -avalanches distributions, whose exponents change with  $p$  (Tab. III). In particular, the  $S$ -avalanche exponent is larger than the  $M$ -avalanche exponent, that is to say the probability to have big  $S$  avalanches is smaller than that to have big  $M$  avalanches. One possible reason for the difference between the two exponents could reside in the observation that  $M$  sites cannot be nearest neighbours, contrarily to  $S$  sites, and thus  $M$  avalanches are intrinsically longer.

We point out that the presence of long range temporal correlations is not necessary for the model to have self-similar or self-affine spatial properties, as already observed in a different context [26].

Our model is a discretized cellular automata which can be thought as a modified version of the Sneppen model for quenched interface growth. The Sneppen model has been shown to be, at least in  $1+1$  dimensions, in the same universality class of the continuous Kardar Parisi Zhang equation with quenched noise [24]. It is natural, but not necessarily true, to suppose that for our model, too, it is possible to find a formulation as a continuous growth equation. Given a general growth equation for  $h(x, t)$  like:

$$\frac{\partial h(x, t)}{\partial t} = A[h(x, t)] + \gamma(x, t) \quad (7)$$

where  $A[\dots]$  is an operator acting on  $h(x, t)$  and  $\gamma(x, t)$  is

an uncorrelated noise, if the operator  $A[\dots]$  is linear and local, the equation can be Fourier transformed into

$$i\omega \tilde{h}(k, \omega) = \tilde{A}(k) \tilde{h}(k, \omega) + \tilde{\gamma}(k, \omega), \quad (8)$$

and by introducing the propagator  $G(k, \omega)$ ,

$$\tilde{h}(k, \omega) = G(k, \omega) \tilde{\gamma}(k, \omega). \quad (9)$$

where  $G(k, \omega) = [i\omega - \tilde{A}(k)]^{-1}$ . For example, the well known Quenched Edward-Wilkinson (QEW) equation [3]:

$$\frac{\partial h(x, t)}{\partial t} = \nu \nabla^2 h(x, t) + \gamma(x, t) \quad (10)$$

has a propagator

$$G(k, \omega) = (i\omega + \nu k^2)^{-1}$$

The propagator  $G(k, \omega)$  of eq. 7 is related to the power spectrum  $S(k)$  of the interface in the asymptotic state. The power spectrum is so defined:

$$S(k) = \langle FT[h(x)h(x')] \rangle = \langle |\tilde{h}(k)|^2 \rangle \quad (11)$$

where  $FT[\dots]$  is the Fourier transform operator, the average is over different realizations of the noise,  $h(x) = h(x, t = \infty)$ ,  $\tilde{h}(k)$  is the Fourier transform of  $h(x)$ . Eq. 11 is valid in the case the noise is uncorrelated in space and time, which is the case of our model. The relation between  $\tilde{G}(k, \omega)$  and  $S(k)$  is the following ([3]):

$$\tilde{G}(k, \omega = 0)^2 = S(k) \quad (12)$$

Equation (12) tells us that the power spectrum of the interface can give informations on  $k$ -dependent part of the propagator  $G(k, \omega = 0)$  and consequently on the structure of the operator  $\tilde{A}(k)$  in Eq. 8. In Figg. 19, 20 we show the behavior of the power spectrum  $S(k)$  of the interface profile in the critical state for system sizes  $L = 2048, 8192$  and different values of  $p$ . The  $S(k)$  follows in the intermediate  $k$  regime a power law

$$S(k) = G(k, \omega = 0)^2 \propto k^{-2\delta}. \quad (13)$$

where we assumed  $G(k, \omega = 0) \propto k^{-\delta}$ . For big values of  $k$  finite size effects connected to the discretized nature of the model become relevant and there is a deviation from the power law behavior. In Tab. IV we report the values of  $\delta$  for different values of  $p$  and for the two different systems sizes  $L = 2048, 8192$ . For  $p = 0.0$  we get  $\delta = 1.86(4)$  ( $L = 8192$ ), which is quite near to the value  $\delta = 2.0$  one gets for the QEW equation [3]. The exponent decreases as  $p$  is increased and for  $p = 0.5$  (the limit for which one should recover Sneppen B model [7]) we get  $\delta = 1.07(3)$  ( $L = 8192$ ). Since Sneppen B model is a cellular automaton and not a continuous equation, it is not straightforward to give an interpretation of the value

$\delta = 1.08(2)$ . However, the Kardar Parisi Zhang equation with quenched noise, which is equivalent to Sneppen model B, has the following form [24]:

$$\frac{\partial h(x, t)}{\partial t} = \nu \nabla^2 h(x, t) + \frac{\lambda}{2} |\nabla h(x, t)| + \gamma(x, t) \quad (14)$$

This equation is characterized by a strong coupling ( $\lambda \gg 1$ ) fixed point, where the linear term becomes dominant and cannot be treated as a small perturbation to the diffusive term. This corresponds to an exponent  $\delta = 1$  in  $G(k, \omega = 0)$ , in the asymptotic self-organized critical state, in good agreement with the numerical findings.

From these results we have a confirmation of the non-universal roughening properties of our model. Actually we are studying the possibility of writing a general continuous equation which shares the same properties of our cellular automata model.

#### IV. EXPERIMENT

In ref. [13] a small-scale experiment of chemical etching on crystalline silicon was performed, in order to check the reliability of our model and in particular of its main outcome: the non universality of the roughness exponent  $\chi$ . We refer the reader to [13] for the details on the setup of the experiment. Here we will only briefly sketch the results. Most of the quantities we have studied numerically could not be reproduced with the experimental setup of [13], but it has been possible to study the roughness property of the surface of the samples after the transient. The most important outcome is the non-universal character of the roughness experiment of the surfaces produced with different degrees of anisotropy. The degree of anisotropy can be related, at its turn, to the temperature and to the environment, so it should depend on the etchants [16,17,25].

The overall effect of the etching process has been the production of pyramidal structures on the interface whose dimensions depend on the anisotropy of the process, on the etchant concentration, on the presence or not of ultrasound agitation, on the temperature and on the time the etching process has gone on.

In [13] the roughness of the surfaces was studied, by analyzing the behavior of the root mean square  $W(l)$  as a function of the length  $l$  of the sample. The results for the roughness seemed to support a non-universal behavior of the roughness, as the experimental parameters (etchant concentration, degree of agitation) were tuned.

Unfortunately, as we pointed out at the beginning of this section, the set up of the experiment in [13] (due to facilities limitations) did not allow for a really quantitative study. We are still waiting for better experiments which could for example allow to relate the experimental conditions (etchant concentration etc.) to the phenomenological parameter  $p$  of our model.

#### V. CONCLUSIONS

In this paper we have introduced a model for surface roughening whose main peculiarity is that of taking explicitly into account the anisotropy of the growth process by means of a tunable phenomenological parameter  $p$  which introduces local, i.e. dependent on the local environment, dynamical rules in the growth. The simple introduction of just one anisotropy parameter  $p$  is far from being able to capture *all* the characteristics of etching processes, and in general of surface roughening experiments. In etching experiments, for example, transport phenomena in the solution are likely to be important and both concentration and agitation have strong effects on transport. Nevertheless, our model captures at least some basic elements of the relationship between anisotropy and the non-universality in etching processes. Moreover, the general requirement of a microscopic dynamical rule depending on the local environment could be a key element in the observed non-universality in kinetic roughening phenomena.

The model exhibits a strong non-universal behavior. For each value of the anisotropy factor  $p$  the system reaches a critical stationary state with a different roughness exponent and a power-law distribution of avalanches. We believe that this behavior is the outcome of the complex interplay between the global dynamics which selects at each time step the weakest site and the anisotropy effect which takes into account local constraints in the growth.

It is worthwhile to stress how our model suggests the possibility of several analytical approach, from the treatment of the problem in terms of a continuous stochastic dynamical equation, to the single site mean-field approach [27], or to the application of a method recently proposed for dynamical models driven by an extremal dynamics [21–23,28]. Particularly promising, in this respect, is a recently proposed non-perturbative Renormalization Group approach [29] which allows one to study self-affine problems.

---

- [1] P. Bak, C. Tang and K. Wiesenfeld, *Phys. Rev. Lett.* **59**, 381 (1987).
- [2] M. Paczuski, P. Bak and S. Maslov, *Phys. Rev. E* **53**, 414 (1996).
- [3] see e.g. the exhaustive review, T. Halpin-Healy and Y.-C. Zhang, *Phys. Rep.* **254**, 215-414 (1995) and references therein.
- [4] G.B. Bales, A.C. Redfield and A. Zangwill, *Phys. Rev. Lett.* **62**, 776 (1989).
- [5] G. Kahanda, X. Zan, R. Farrell and P.-Z. Wang, *Phys. Rev. Lett.* **68**, 3741 (1992).

- [6] M. Kardar, G. Parisi and Y.-C. Zhang, *Phys. Rev. Lett.* **56**, 889 (1986).
- [7] K. Sneppen, *Phys. Rev. Lett.* **69**, 3539 (1992).
- [8] L.H. Tang and H. Leschhorn, *Phys. Rev. A* **45**, R8309 (1992), and T. Nattermann, S. Stepanow, L.H. Tang and H. Leschhorn, *J. Phys. II France* **2**, 1483 (1992).
- [9] B. Sapoval, S. B. Santra and Ph. Barboux, *Europhys. Lett.* **41**, 297 (1998); A. Gabrielli, A. Baldassarri and B. Sapoval, preprint cond-mat/0002298.
- [10] J. Zhang, Y.-C. Zhang, P. Alstrom and M. T. Levinsen, *Physica* **A189**, 383 (1992).
- [11] M. A. Rubio, C. A. Edwards, A. Dougherty and J. P. Gollub *Phys. Rev. Lett.* **63**, 1685 (1989).
- [12] V.K. Horvath, F. Family and T. Vicsek, *Phys. Rev. Lett.* **65**, 1388 (1990).
- [13] R. Cafiero, V. Loreto and P. Prosin, *Europhys. Lett.* **42**, issue 4, 389-394 (1998).
- [14] E. Yablonovitch and G. D. Cody, *IEEE Transactions on Electron Devices* **ED-29**, 300 (1982).
- [15] H. Seidel, L. Csepregi, A. Henberger and H. Boumgartel, *J. Electrochem. Soc.* **137**, 3612 (1990).
- [16] M. Elwenspock, *J. Electrochem. Soc.* **140**, 2075 (1993).
- [17] P. Allongue, V. Costa-Kieling and H. Gerischer, *J. Electrochem. Soc.* **140**, 1009 (1993) and **140**, 1018 (1993).
- [18] V. Loreto, A. Vespignani and S. Zapperi, *J. Phys. A* **29**, 2981 (1996).
- [19] J. M. Kim and J. M. Kosterlitz, *Phys. Rev. Lett.* **62**, 2289 (1989).
- [20] S. Maslov, *Phys. Rev. Lett.* **74**, 562 (1995).
- [21] M. Marsili, *Europhys. Lett.*, **28**, 385 (1994).
- [22] A. Gabrielli, R. Cafiero, M. Marsili and L. Pietronero, *Europhys. Lett.*, **38** (7), pp.491-496 (1997).
- [23] R. Cafiero, A. Gabrielli, M. Marsili and L. Pietronero, *Phys. Rev. E* **54**, 1406 (1996).
- [24] G. Parisi, *Europhys. Lett.* **17**, 673 (1992).
- [25] D.L. King and M. Elaine Buck, 23th IEEE PVSC, (1991), pp.303-308.
- [26] A. Gabrielli, R. Cafiero, and G. Caldarelli, *Europhys. Lett.* **45** (1), 13-19 (1999).
- [27] R. Dickman, *J. Stat. Phys.* **55**, 997 (1989).
- [28] M. Marsili, *J. Stat. Phys.* **77**, 733 (1994); A. Gabrielli, M. Marsili, R. Cafiero and L. Pietronero, *J. Stat. Phys.* **84**, 889-893 (1996).
- [29] C. Castellano, M. Marsili and L. Pietronero, *Phys. Rev. Lett.* **80**, 4830 (1998).

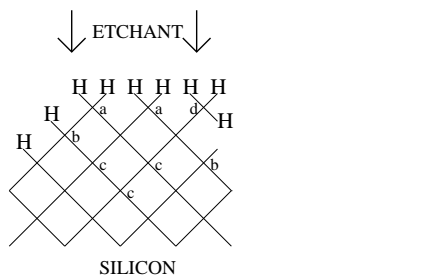


FIG. 1. Schematic representation of the crystalline silicon lattice as a square lattice.

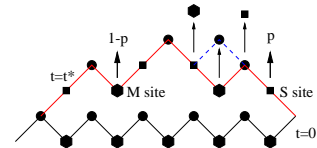


FIG. 2. Schematic representation of interface dynamics.

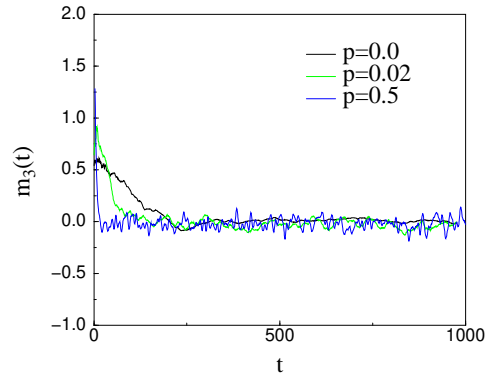


FIG. 3. Time evolution of the moment  $m_3$  of the growing interface, normalized by the second moment, for  $p = 0.0, 0.02, 0.5$  (skewness). One sees that asymptotically  $m_3$  vanishes for all values of  $p$ .

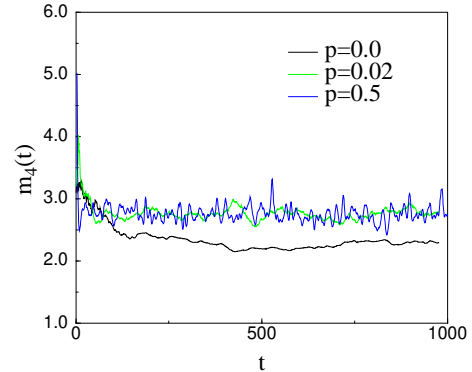


FIG. 4. Time evolution of the moment  $m_4$  of the growing interface, normalized by the second moment, for  $p = 0.0, 0.02, 0.5$ . One sees that asymptotically  $m_4$  tends to different constant values for the different values of  $p$ .

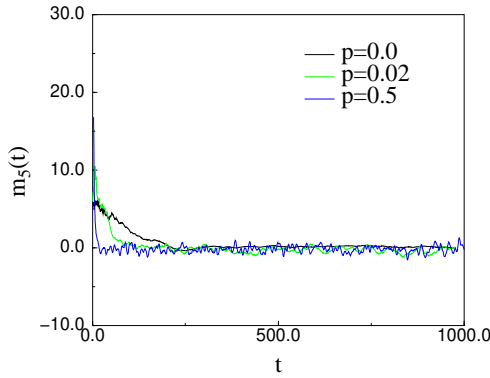


FIG. 5. Time evolution of the moment  $m_5$  of the growing interface, normalized by the second moment, for  $p = 0.0, 0.02, 0.5$ . One sees that asymptotically  $m_5$  vanishes for all values of  $p$ .

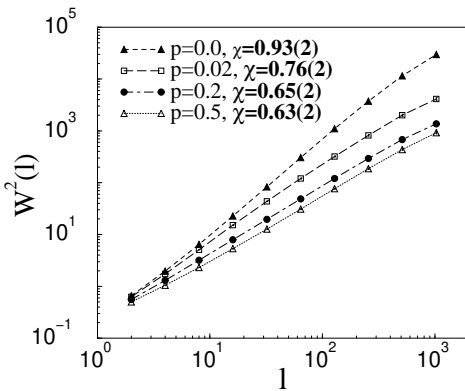


FIG. 6. Scaling behavior of  $W^2(l)$  in the framework of our model for different values of  $p$ .  $L = 2048$ , total evolution time  $t = 10^7$  steps.

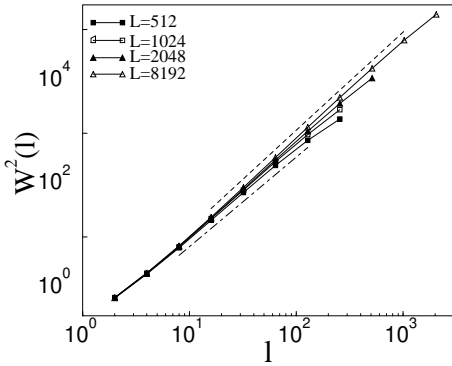


FIG. 7. Power law fit of  $W^2(l)$  for  $p = 0.0$  and growing system size. The lower fit (dot-dashed line) corresponds to a size  $L = 512$ , giving an exponent  $\chi = 0.88(2)$ , while the upper fit (dashed line) corresponds to a size  $L = 8192$  and gives an exponent  $\chi = 0.96(2)$ .

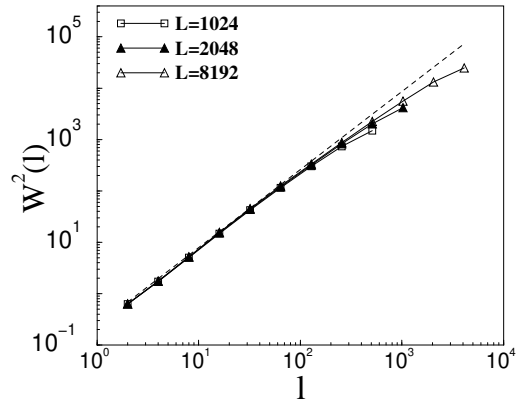


FIG. 8. Power law fit of  $W^2(l)$  for  $p = 0.02$  and growing system size. A power law fit (dashed line) gives an exponent  $\chi = 0.76(2)$ .

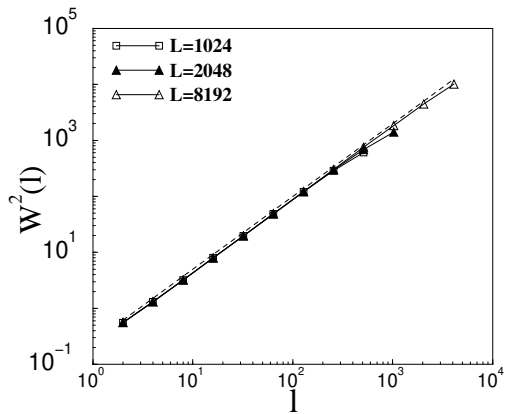


FIG. 9. Power law fit of  $W^2(l)$  for  $p = 0.2$  and growing system size. A power law fit (dashed line) gives an exponent  $\chi = 0.65(2)$ .

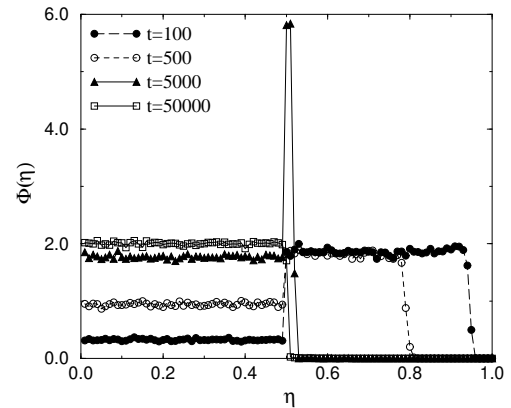


FIG. 10. Histogram  $\Phi(\eta)$  of quenched variables, at different times  $t$ , for  $p = 0.0$ . Asymptotically, all (most of the)  $M$  variables are eliminated.

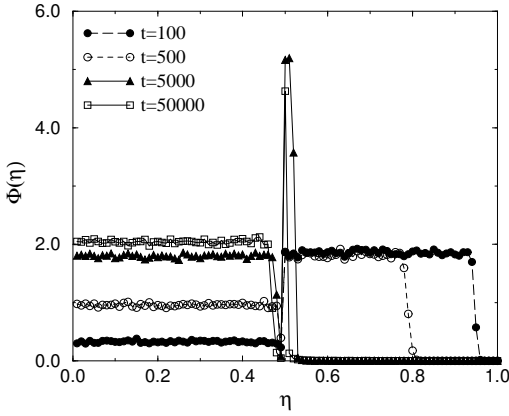


FIG. 11. Histogram  $\Phi(\eta)$  of quenched variables, at different times  $t$ , for  $p = 0.02$ .

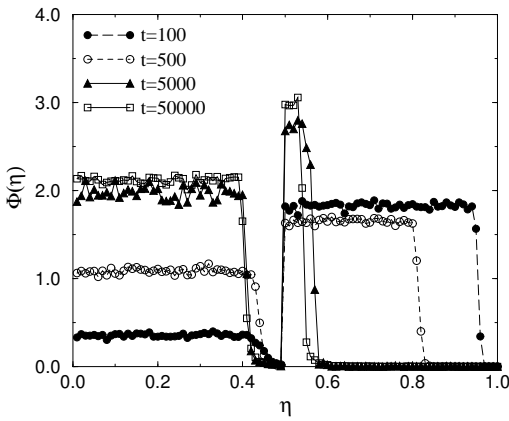


FIG. 12. Histogram  $\Phi(\eta)$  of quenched variables, at different times  $t$ , for  $p = 0.2$ .

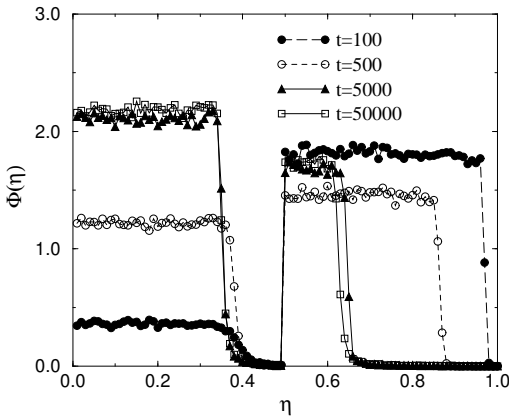


FIG. 13. Histogram  $\Phi(\eta)$  of quenched variables, at different times  $t$ , for  $p = 0.5$ .

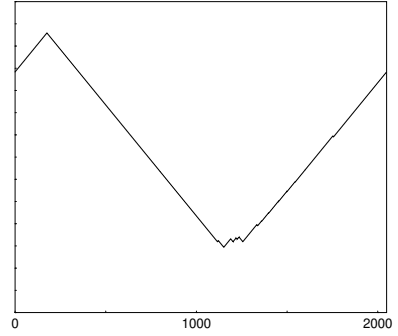


FIG. 14. A realization of the growing surface for  $p = 0.0$  (horizontal length on the  $x$  axis). The surface is composed by very big pyramids, thus with a strong prevalence of  $S$  sites.

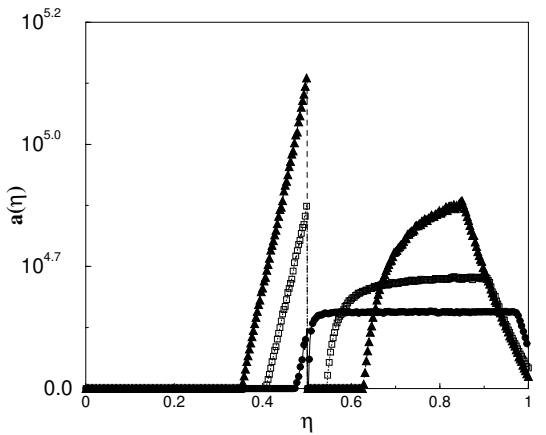


FIG. 15. Asymptotic acceptation (not normalized) profile  $a(x)$  for  $p = 0.02$  (circles),  $p = 0.2$  (squares) and  $p = 0.5$  (triangles).

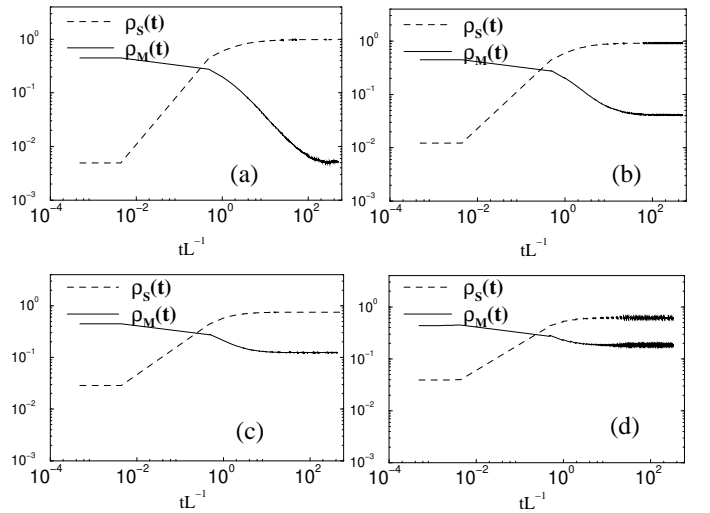


FIG. 16. Time evolution of the densities  $\rho_S$  and  $\rho_M$  of sites  $S$  and  $M$  respectively, for  $p = 0.0$  (a),  $p = 0.02$  (b),  $p = 0.2$  (c), and  $p = 0.5$  (d).

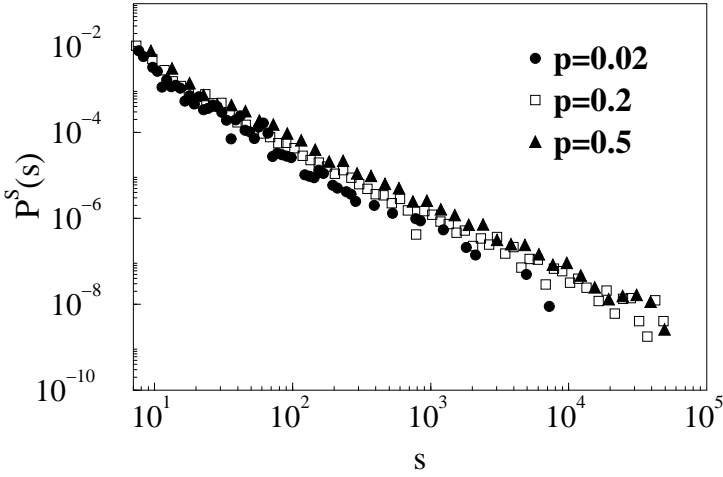


FIG. 17. Binned S-avalanches distribution for different values of  $p$ .

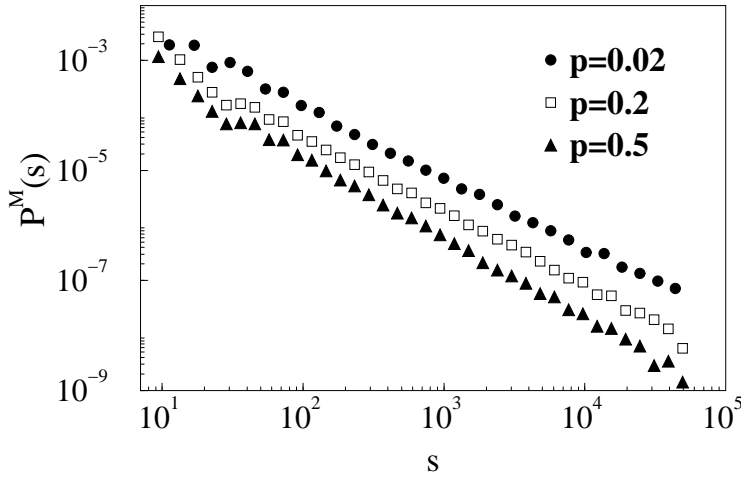


FIG. 18. Binned M-avalanches distribution for different values of  $p$ .

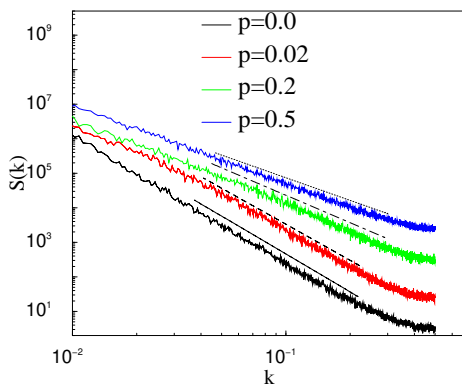


FIG. 19. Power spectrum  $S(k)$  of our model for  $p = 0.0, 0.02, 0.2, 0.5$  (values referring to, respectively, the plots from bottom to top) and  $L = 2048$  together with a power law fit (the corresponding values of  $\delta$  are reported in Table. IV).

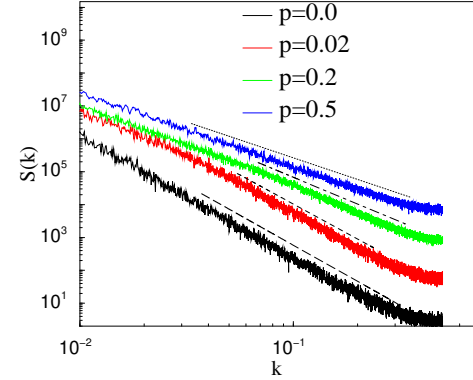


FIG. 20. Power spectrum  $S(k)$  of our model for  $p = 0.0, 0.02, 0.2, 0.5$  (values referring to, respectively, the plots from bottom to top) and  $L = 8192$  together with a power law fit (the corresponding values of  $\delta$  are reported in Table. IV).

TABLE I. Values of the roughness exponent  $\chi$  and of the dynamical exponent  $\beta$  in our model for different values of the anisotropy parameter  $p$ .

$p$	$\chi$	$\beta$
0.0	0.93(2)	0.96(2)
0.02	0.76(2)	0.95(2)
0.2	0.65(2)	0.94(2)
0.5	0.63(2)	0.95(2)

TABLE II. Critical thresholds  $\eta_c^S, \eta_c^M$  of variables  $S$  and  $M$ , for different values of  $p$ .

$p$	$\eta_c^S$	$\eta_c^M$
0.02	0.47(1)	0.50(1)
0.2	0.41(1)	0.54(1)
0.5	0.35(1)	0.63(1)

TABLE III.  $S$  and  $M$  avalanche distribution exponents  $\tau_S$  and  $\tau_M$ , for different values of  $p$ .

$p$	$\tau_S$	$\tau_M$
0.02	1.8(1)	1.29(3)
0.2	1.65(4)	1.36(3)
0.5	1.50(4)	1.48(3)

TABLE IV. Values of the exponent  $\delta$  of the power spectrum  $S(k)$ , for different values of  $p$  and  $L = 2048, 8192$ .

$p$	$L = 2048$	$L = 8192$
0.0	1.85(4)	1.86(3)
0.02	1.75(4)	1.77(3)
0.2	1.32(4)	1.35(3)
0.5	1.08(4)	1.07(3)